Resources, Conservation & Recycling 188 (2023) 106647

Contents lists available at ScienceDirect

Resources, Conservation & Recycling

journal homepage: www.elsevier.com/locate/resconrec

Resource mining from stainless steel pickling wastewater to produce metal-organic frameworks

Xudong Zhao [a], Chengwei Zhang [a], Baosheng Liu [b,*], Huifang Zhao [c], Xinli Gao [d], Yuanyang Wang [a], Yuezhong Zhang [a], Dahuan Liu [c,*], Chong-Chen Wang [e,*]

[a] College of Chemical and Biological Engineering, Taiyuan University of Science and Technology, Taiyuan 030024, China
[b] College of Materials Science and Engineering, Engineering Research Center for Magnesium Alloy of Shanxi Province, Taiyuan University of Science and Technology, Taiyuan 030024, China
[c] State Key Laboratory of Organic-Inorganic Composites, College of Chemical Engineering, Beijing University of Chemical Technology, Beijing 100029, China
[d] Instrumental Analysis Center, Taiyuan University of Science and Technology, Taiyuan 030024, China
[e] Beijing Key Laboratory of Functional Materials for Building Structure and Environment Remediation, Beijing University of Civil Engineering and Architecture, Beijing 100044, China

ARTICLE INFO

Keywords:
Stainless steel pickling wastewater
Metal-organic framework
Selective crystallization
Resource recycling

ABSTRACT

Metal-organic frameworks (MOFs) exhibit large potential in many fields while the high cost limits their large-scale use. Herein, stainless steel pickling wastewater was successfully transformed to Fe/Cr-MIL-100, during which Ni^{2+} was largely purified. As an integration of metal, solvent and acid modifier, the use of the wastewater simplifies the preparation units and reduces the cost of MOFs. Conversion of the pickling wastewater to MOFs is feasible under wide reaction conditions and is not interfered by discharge batch of the wastewater. The obtained MIL-100 s products exhibit excellent porosity, long-term acid/base stability, and large adsorption capacities for methylene blue, moxifloxacin hydrochloride, and zirconium (IV) ion. Thus, our work provides a new insight for effective reuse of industrial wastewater and a feasible method for reducing MOFs cost.

1. Introduction

During the past two decades, metal-organic frameworks (MOFs) have emerged huge potentials in many fields such as catalysis, separation, degradation and chemical sensing (Zeng et al., 2021; Xia et al., 2021; Fathieh et al., 2018; Razavi and Morsali, 2020), whereas relatively higher cost than zeolite and carbon-based materials seriously limits their industry-level use. Raw materials of MOFs involve metal source, organic ligand, solvent, and acid/base modifier agent (if needed), substitution of which by industrial wastes will effectively reduce the cost. In the past years, some industrial metal wastes have been conversed to high value-added MOFs (Perez et al., 2016; Vo et al., 2019; Kabtamu et al., 2020; Song et al., 2021). Therein, the attempts based on metal wastewater were also reported. For example, simulated battery waste liquor and waste hexavalent chromium solution were used to prepare MOFs (Perez et al., 2016; Vo et al., 2019). However, these attempts were commonly carried out based on the simulated wastewater. Up to date, conversion of practical industrial wastewater to highly valuable MOFs was rarely reported.

Stainless steel manufacturing industry is distributed worldwide and exhibits an increasingly huge annual output. The operation unit of oxide skin pickling will produce a mass of wastewater, which contains high concentrations of Fe^{3+}, Cr^{3+}, Ni^{2+}, F^{-}, NO_3^{-} and possesses strong acidity (Rögener et al., 2012). The reuse and recovery of the metals and acids in the pickling wastewater can reduce pollution caused by wastewater discharge, and facilitate the resource recycle. Recently, some conversion attempts have been made based on this wastewater (Yi et al., 2021; Yang et al., 2019; Hermose et al., 2005; Zhang et al., 2021), while the added values of the formed products are not very high and importantly, the treatment of the secondary wastewater and formed hazardous waste still faces challenges. Excitingly, we noted that the metal ions, acids (HF and HNO_3), and water of the stainless steel pickling wastewater correspond to all the raw materials of MOFs except for organic ligands. Use of this raw-material integration will largely simplify the preparation units and reduce the cost of MOFs.

In this work, a 3R (reduce, reuse, recycle) approach for treating stainless steel pickling wastewater was proposed, based on the selective crystallization reaction with 1,3,5-benzenetricarboxylic acid (H_3BTC).

* Corresponding authors.
E-mail addresses: baoshengliu@tyust.edu.cn (B. Liu), liudh@mail.buct.edu.cn (D. Liu), wangchongchen@bucea.edu.cn (C.-C. Wang).

https://doi.org/10.1016/j.resconrec.2022.106647
Received 30 April 2022; Received in revised form 6 August 2022; Accepted 5 September 2022

Fe^{3+} and Cr^{3+} participate preferably to the reaction to form Fe/Cr-mixed MIL-100 materials and meanwhile Ni^{2+} was largely purified, realizing the reuse and discharge reduction of the pickling wastewater and the recycle of metal/acid resources. The topology structure, porosity, long-term acid/base stability, and water-phase adsorption performances of the obtained MOFs were systematically measured and analyzed. To the best of our knowledge, the conversion of stainless steel pickling wastewater to MOFs is firstly reported by this work. Our work will promote recycle of industrial wastes resource and large-scale use of MOFs.

2. Experimental section

2.1. Materials

The stainless steel pickling wastewater was collected from Sinosteel Stainless Steel Pipe Technology (Shanxi) Co., Ltd. (Fig. S1). The wastewater shows the dark green colour and its compositions are listed in Table S1. 1,3,5-Benzenetricarboxylic acid (H_3BTC), N,N'-dimethylformamide (DMF), methylene blue (MB), methyl orange (MO), moxifloxacin hydrochloride (MOX), zirconium oxychloride octahydrate ($ZrOCl_2{\cdot}8H_2O$) were purchased from HWRK Chem. Co., Ltd.

2.2. Synthesis of MOFs

Herein, MOFs were synthesized according to a simple hydrothermal method. The pickling wastewater (20 mL) and H_3BTC ligand (1, 2, 3, and 5 g) were mixed and stirred for 5 min (solid/liquid ratio: 50, 100, 150 and 250 g/L). After that, the mixture was transferred into a 100 mL stainless steel lined reactor and heated for 12 h at 180~220 °C. After being cooled down to room temperature, the solid was collected and further washed with DMF and deionized water. Also, ethanol with low-toxicity was also attempted to replace DMF and the results were presented in subsequent discussions. At last, the solid was dried at 100 °C overnight. The samples were named as BTC-X-Y, where X is the solid/liquid ratio and Y is the reaction temperature. The detailed reaction conditions are listed in Table S2.

In this work, we collected three batches of pickling wastewater and it is noted that if no special reminder, the samples were prepared with the 1st batch of wastewater.

2.3. Characterization methods

The powder X-ray diffraction (XRD) patterns of BTC-X-Y samples were measured on a D8 Advance X diffractometer with Cu Kα radiation. N_2 adsorption-desorption isotherms at 77 K were measured on a PSD-PS2 surface area analyzer and desolvation temperature was set at 120 °C. The morphology was characterized using a SU8020 field emission scanning electron microscope (SEM). The composition and elements distribution were measured on a scanning electron microscope (TESCAN MIRA LMS) equipped with an energy dispersive X-ray system (Xplore). Infrared spectra were collected on a Nicolet iS50 FTIR spectrophotometer. X-ray photoelectron spectra (XPS) was obtained on an Axis Supra X-ray photoelectron spectroscope, and Al Kα X-ray excitation source was selected. The compositions of organic elements were measured on an elemental analyzer (Elementar Vario El III).

2.4. Adsorption experiments

The BTC-X-Y sample (10 mg) was added into the aqueous solutions (10 mL) of MOX, MB and Zr(IV) ions and well mixed. Then, the mixture was stirred in a constant temperature shaker at 303 K for 12 h. After that, clear filtrate was collected through membrane filtration. The concentrations of MOX and MB were analyzed on a UV–Vis spectrometer (TU-1901, Persee) and that of Zr(IV) ion was measured on an inductively coupled plasma optical emission spectrometer (ICP-OES, Avio 200). The adsorption amount was calculated according to following equations:

$$Q = \frac{(C_0 - C_e) \times V}{m} \quad (1)$$

where C_0 (mg/L) and C_e (mg/L) are the concentrations of solutes before and after adsorption respectively, V (L) is the volume of aqueous solution and m (g) is the MOF mass, Q (mg/g) is the adsorption amount.

3. Results and discussion

3.1. Preparation and characterization of the products

The preparation process of BTC-X-Y is shown in Scheme 1. The pickling wastewater and H_3BTC were used as the total raw materials and on other additional reagents were added. A simple hydrothermal reaction was carried out and the earthy-yellow powders were collected. As an integrated body of metal, solvent and acid, use of the pickling wastewater simplifies the operation units of MOF preparation and promotes the green synthesis of MOFs.

As shown in Fig. 1a–c, the powder XRD patterns of BTC-X-Y samples are almost consistent with simulated XRD pattern of standard MIL-100 crystal. Some additional diffraction peaks for unknown phases appear in the patterns of BTC-50-220 and BTC-100-220. Thus, under the solid/liquid ratio of 50–250 g/L and temperature of 180–220 °C, the crystal topology belongs to MIL-100 structure (Fig. 1d). Besides, other temperatures were also tried. Lower temperature (160 °C) will limit the formation of product due to the decreased reaction activity and higher temperature (240 °C) results in some black amorphous powders for possible carbonization phenomenon. Concluded above, MIL-100 crystals can be obtained at the wide reaction conditions, which benefits to practical production of MOFs.

Due to the complexity of real pickling wastewater, some unknown by-products without characteristic XRD peaks may also exist. Besides, from the view of industrial production, the purity of products is an important indicator to be concerned. Herein, we calculated the carbon-based purity according to the theoretical and experimental contents of carbon component. In the classical reports about MIL-100 s (Férey et al., 2004; Horcajada et al., 2007), the formula of MIL-100 was defined as $M_3F(H_2O)_2O(BTC)_2{\cdot}(H_2O)_n$. In our work, the MIL-100 crystals can be described as $(Fe_xCr_y)_3F_z(H_2O)_{3-z}O(BTC)_2{\cdot}(H_2O)_n$. To rationally determine the purity, the interference of free H_2O (n H_2O) was eliminated via a dehydration process. As reported in Horcajada et al. work (Horcajada et al., 2007), free H_2O was removed at ~80 °C and thereby the formula of the thermally treated products can be simplified as $(Fe_xCr_y)_3F_z(H_2O)_{3-z}O(BTC)_2$. The values of x, y, z, theoretical formula weights and C content were listed in Table S3. All the products exhibit a roughly close value of formula weight (651 g/mol) and C content (33.1 wt%). The real C contents were determined via elemental analysis (EA) measurement and were found to be slightly higher than the theoretical values. The purities were calculated and exhibited large values of 95.0~98.9% (Table 1). Due to the existence of additional crystal phases, BTC-50-220 and BTC-100-220 were not considered. Besides, the yields based on BTC ligand were also calculated. The highest conversion efficiency was found at the solid/liquid ratio of 100 g/L and the lowest values were at 250 g/L due to excessive BTC usage.

In the FTIR spectra (Fig. S2–S4), the peaks for C—H are assigned to benzene ring of BTC ligand, and the presence of carboxylate ($-COO^-$) confirms the coordination between BTC ligands and the metal ions (Valenzano et al., 2011). The permanent porosity of the BTC-X-Y was evaluated via N_2 adsorption-desorption isotherms at 77 K (Fig. 2). The total pore volumes of the products range from 0.65~1.01 cm^3/g and the Brunauer-Emmett-Teller (BET) specific surface areas reach 1127.3~1865.8 m^2/g (except for BTC-50-220), comparable with the MIL-100 s prepared by traditional methods (Table S4) (Jing et al., 2021; Dhakshinamoorthy et al., 2011; Guo et al., 2020; Huo and Yan, 2012; Hasan et al., 2012; Bezverkhyy et al., 2016; Plaza et al., 2012; Jhung

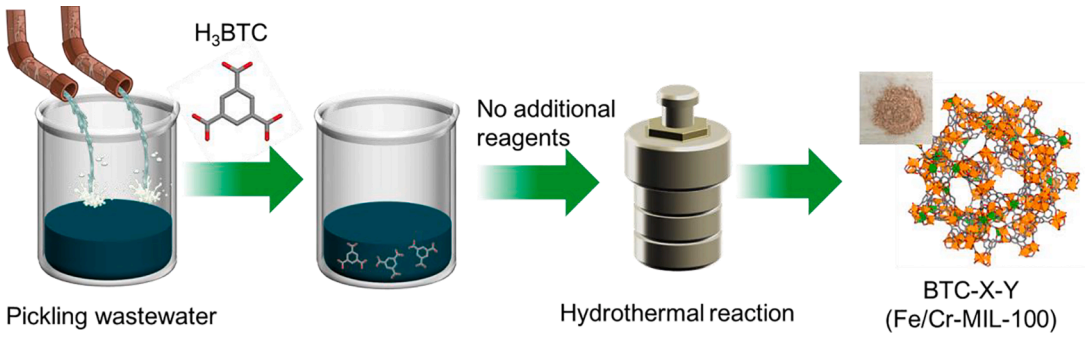

Scheme 1. The preparation process of BTC-X-Y based on the hydrothermal reaction of H_3BTC and pickling wastewater.

Table 1
The purity, yield, pore characteristics, and elemental contents of the samples.

BTC-sample	Purity[a] (%)	Yield[b] (%)	S_{BET}[c] (m^2/g)	V_p[d] (cm^3/g)	d[e] (nm)	Fe/Cr[f]	(Fe+Cr)/F[f]
BTC-50-180	98.6	85.1	1146.6	0.6547	0.7, 1.1, 1.6	12.0	4.8
BTC-100-180	95.8	97.2	1387.3	0.7463	0.7, 1.2, 1.8	9.5	3.3
BTC-150-180	98.9	78.0	1358.1	0.8115	0.5, 1.1, 1.6	6.7	3.5
BTC-250-180	95.6	53.5	1341.2	0.8733	0.5, 1.1, 1.5	6.3	2.9
BTC-50-200	95.9	61.0	1355.0	0.8282	0.5, 1.1, 1.6	7.5	2.5
BTC-100-200	96.9	97.9	1173.6	0.7617	0.5, 1.1, 1.6	7.5	3.1
BTC-150-200	95.6	64.9	1336.1	0.7110	0.8, 1.2, 1.7	6.7	5.1
BTC-250-200	98.0	51.8	1366.6	0.8773	0.6, 1.1, 1.6	5.4	4.6
BTC-50-220	—	—	562.1	0.5365	0.6, 1.1, 1.6	2.8	2.7
BTC-100-220	—	—	1127.3	0.6894	0.8, 1.3, 1.7	5.5	1.3
BTC-150-220	97.8	73.1	1572.5	0.9255	0.8, 1.2, 1.7	4.7	1.7
BTC-250-220	95.0	60.8	1865.8	1.0163	0.7, 1.2, 1.7	4.6	2.8

[a] The purity was calculated based on carbon contents in theory and experiment and the detailed calculation method was shown in Supporting Information.
[b] The yield was based on BTC ligand.
[c] S_{BET} is the Brunauer-Emmett-Teller (BET) specific surface area.
[d] V_p is the total specific pore volume determined by using the adsorption branch of the N_2 isotherm at $P/P_0 = 0.99$.
[e] d is the pore diameter determined by the density functional theory (DFT) method.
[f] The ratio refers to molar ratio.

et al., 2005; Wickenheisser et al., 2013; Hamon et al., 2012; Long et al., 2011; Tong et al., 2013). The pore size distributions results based on DFT method (Fig. S5–S7) show the pore ranges of 0.5~1.8 nm. Thus, the high porosity of the BTC-X-Y is confirmed. Furthermore, in the activation process of the products, we tried to substitute DMF solvent by lower-toxicity ethanol. Due to the high solubility of the metal ions and H_3BTC ligands in this solvent, the ethanol-treated samples also exhibit high porosity (Fig. S8), only slightly lower than that of DMF-treated samples. Thus, ethanol can also serve as a feasible solvent for the products activation.

The morphology and particles sizes of the BTC-X-Y samples were observed via SEM images (Figs. S9–S11). Taking BTC-250-180, BTC-50-200 and BTC-150-220 as examples (Fig. 3a–c), the samples consist of octahedrons and some irregular particles with the size of 0.5–1 μm. Element compositions of the products were investigated via SEM-EDS analysis (Fig. 3d–o, S12–S14). The BTC-X-Y samples consist of Fe, Cr, F, C and O elements, and Ni and N (from NO_3^-) elements are not found. This may be attributed to the weaker coordination ability of Ni^{2+} and NO_3^- with H_3BTC linker and Fe/Cr sites respectively. Besides, we found the concentrations of Fe and Cr in the wastewater were obviously decreased after the reaction and that of Ni kept almost unchanged (Table S2). From the high-resolution XPS patterns (Fig. S15a-S15c), the signs of F 1 s locate at 684–687 eV, confirming the formation of Cr-F and Fe-F bonds (Gross and Treu, 2008; Carraro et al., 2013). The small difference of binding energy for the samples may be attributed to the different Fe/Cr ratios. So, the Fe/Cr-mixed inorganic cluster with bonded F is verified, as shown in Fig. S15d.

Furthermore, as listed in Table 1, the molar ratio of Fe and Cr ranges ~5–12 (the case of BTC-50-220 are excluded). Herein, the Fe/Cr ratio seems to be not very consistent with the concentration change of metal ions in pickling wastewater. This issue was investigated and analyzed in Section 3.5. Besides, we found the Fe/Cr ratio follows a rough rule: the ratio is lower under the higher temperature and solid/liquid ratio. The possible reason was explained as follows. MIL-100-Fe/Cr is formed via the reaction of the Lewis acid (Fe^{3+}/Cr^{3+}) and the Lewis base (BTC_3^- linker). As proved by previous reports (Tong et al., 2013; Lian et al., 2015), Cr-MOFs are more stable than Fe-MOFs with sample topology. (i) Under lower temperature, the reactivity of Fe^{3+} and Cr^{3+} are relatively lower and Fe^{3+} with large proportion tends to be reacted. Under higher temperature, Fe^{3+} and Cr^{3+} are both more easily to be reacted but Cr-BTC is easier to be remained in the reaction system due to its higher stability. (ii) Under lower solid/liquid ratio, limited by less reaction sites (BTC amount), Fe^{3+} with large proportion is more likely to participate in the reaction and the reaction probability of Cr^{3+} with small proportion is sharply decreased. Under higher ratio especially for 250 g/L, more BTC linkers provide abundant reaction sites. Fe^{3+} and Cr^{3+} are both likely to react with BTC linkers and their reaction probability tends to be close to the Fe/Cr ratio in the pickling wastewater. Considering the different functions of Fe and Cr sites, this adjustable Fe/Cr ratio will benefit to the practical applications of MOFs. The ratio of total metal and F locates at 1.7–4.8, almost comparable with that (3.0) of standard MIL-100(Fe) or MIL-100(Cr) (Férey et al., 2004; Horcajada et al., 2007). Therefore, the successful transformation of the stainless steel pickling wastewater to Fe/Cr-mixed MIL-100 crystals is demonstrated.

3.2. Stability test

Herein, BTC-X-Y samples were formed under the strongly acid system (pH < 0) and thereby the potential stability is expected. In order to examine the chemical stability of BTC-X-Y, the sample (using BTC-250-180 as example) was immersed in aqueous solutions with wide pH range of 1–12 at room temperature. After 10 days, the samples were collected for XRD and porosity measurement. The main diffraction peaks remain almost unchanged (Fig. 4a), indicating the relatively stable crystal structure. As shown in Fig. 4b, the nitrogen adsorption amount increases obviously after the immersion experiment. The porosity including BET specific surface area and pore volume is enhanced (Table S5). This increase may be attributed to the following reasons: (i) the pores of the sample were activated (or washed) more effectively. In other words, the residual raw materials inside the channel and on the surface were removed more sufficiently. (ii) The acid or base may play an etching action for the MOF, inducing the breakage of a small amount of coordination bonds. This results in the possible formation of defect structures. Thus, the long-term acid/base stability of BTC-X-Y sample was confirmed.

3.3. Preparation by different batches of pickling wastewater

During the production process of plants, the compositions of different batches of wastewater are commonly different with each other due to uncontrollable factors. Thus, from the point of view of long-term industrial production, the feasibility for continuous conversion from pickling wastewater to MOFs was assessed. For that, another two batches of pickling wastewater were collected once two months. As listed in Table S1, the compositions of 2nd and 3rd batches of pickling wastewater are obviously different with that of 1st batch. However, even that, MIL-100 materials with high porosity were still obtained, as shown in Fig. 5a and b. This indicates that formation of MIL-100 is not largely controlled by discharge batch of wastewater and continuous production in industrial-level scale may be feasible.

However, real pickling wastewater still faces some challenges than simulated wastewater. In industry, the mixed acid (pickling liquor) was used to pickle the oxide skins, produced by various treatment technics, for example, smelting, casting, hot rolling, heat treatment and welding. Besides, the acid may also applied for various models of steels. Due to the diverse Fe/Cr contents in different steels or oxide skins, the Fe/Cr concentrations in actual wastewater are various. As described in many works, the functions of Fe and Cr are different in many applications (e.g. adsorption, catalysis, and advanced oxidation). Thus, the MIL-100 products derived from different batches of wastewater may exhibit diverse functions, which may be the main challenge for real wastewater.

3.4. Cost assessment and optimization

In this work, during the synthesis reaction of BTC-X-Y samples, the Fe/Cr metal, reaction solvent, and inorganic acid were substituted by stainless steel pickling wastewater. Thus, cost reduction of the MOFs is highly expected. Besides, in the washing (or activation) step for BTC-X-Y samples, organic solvent and deionized water were used. The costs of these solvents were also considered and the costs were assessed (Table S6). The market prices of the reaction reagents were collected from Macklin Biochemical Co., Ltd and that of DMF was collected from Tianjin Zhiyuan Chemical Reagent Co. Ltd. The very low cost of the pickling wastewater was ignored. However, in the literatures about MIL-100 preparation, the detailed solvent dosage in the activation step was rarely reported. It is difficult to rationally compare the total costs, if considering the solvents used for product activation.

Herein, as a rational comparison, we assessed the MOFs costs based on raw materials only in the synthesis reaction. As shown in Table S6, the costs of the BTC-X-Y samples are determined to 0.135~0.256 $/g. We noted, by and large, that the cost was increased along with the increasing H_3BTC usage, caused by the reducing utilization efficiency of H_3BTC. Meanwhile, the costs of standard MIL-100(Cr) and MIL-100(Fe) prepared by traditional methods (Férey et al., 2004; Hasan et al., 2012) were assessed to 0.354 and 0.357 $/g (Table S7). The cost is reduced by 28~61% compared with MIL-100(Cr) prepared by traditional method. Thus, our method can effectively promote the cost reduction and points out an alternative route to treat stainless steel pickling wastewater.

In the industry of stainless steel production, the mixed acid was used as the pickling liquor. During the successional pickling process, the concentrations of metal ions are increased and meanwhile solution acidity is decreased. Until disabled, this liquor will be discharged. It is important to investigate which extent of pickling use is optimal for the economic costs of relevant enterprises, if applied for MOFs conversion. In the presented system, MIL-100 is formed based on the interaction of BTC Lewis base and Fe^{3+}/Cr^{3+} Lewis acid: $H_3BTC + M^{3+} \rightarrow BTC-M + 3H^+$ (M = Fe or Cr). From the view of reaction equilibrium, higher concentration of metal ions and lower acidity will promote the reaction. From Table S8, the discharged pickling wastewaters from different regions (or factories) show diverse acidity (or pH) but still remain considerable values (Rögener et al., 2012; European Comission, 2001). Under the acidic conditions, the formation of MIL-100 was proved to be feasible by our work. Besides, Fe/Cr-BTCs were coomonly synthesized in an acidic system to obtain high crystallinity, via slowing down reaction rate (Férey et al., 2004; Yoon et al., 2010; Tan et al., 2015). Therefore, the pickling liquor with longer use time (or the totally inactivated liquor) is the best choice for MIL-100 production. This is also a positive aspect for the economic benefit of production enterprises.

3.5. The overall green cycle route and metal flow directions

As described before, the yields (based on BTC ligand) of the products are obviously lower than 100% especially under high solid/liquid ratios. Thus, the treatment of unreacted raw materials and secondary wastewater should be solved, if being industrialized. For that, we proposed some feasible strategies, as presented in Scheme 2.

(i) *Treatment of the secondary wastewater (Solution A)*. As shown in Table S2, after the synthesis reaction, the residual pickling liquor still contains high-concentration metal ions. Higher reaction temperature and solid/liquid ratio lead to lower residues of Fe and Cr, while the concentration of Ni still remains a considerable value compared with the original liquor. Under 220 °C and solid/liquid ratio of 250 g/L, the removal percentages of Fe and Cr reaches maximum values of 84.5% and 95.2% and the purity of Ni reaches ~60.0 wt%, higher than 15.2 wt% of the original liquor. To convert Fe/Cr ions to MOFs more sufficiently and meanwhile improve the purity of Ni, higher solid/liquid ratios (500, 650, 750 g/L) were tried at 220 °C. These higher usages can still result in MIL-100 classes (Fig. S16-S18). Under the ratio of 650 g/L, the removal ratios of Fe and Ni are improved to 97.7% and 99.8%, and the purity of Ni reaches up to 90.7 wt% (Table S9); meanwhile, the colour of pickling wastewater changes from dark green to Ni-characterized light green. Higher solid/liquid ratio (750 g/L) functions not better for the formation of more viscous system that limits the diffusion and mass transfer of the regents. Further, on the basis, a secondary reaction with H_3BTC was performed. Upon this, the residual Fe was almost removed completely (99.4%) and meanwhile transformed to Fe-MIL-100 (Fig. S19), and the content of Ni was purified up to 98.0%. The two-step reaction process and flow directions of Fe, Cr, Ni are presented in Scheme 3.

(ii) *Treatment of the unreacted raw materials*. As shown in Scheme 2, solid-phase sample was collected via centrifugation. Some unreacted H_3BTC ligands were remained in the solid and some unreacted metal ions were also attached. Firstly, the solid mixture was washed with deionized water to remove the attached metal ions, resulting in Solution B. Secondly, ethanol was used to dissolve the ligand, resulting in Solution C. After a simple distillation process, ethanol was volatilized and the residual solid was collected. As presented in Fig. S20, the XRD pattern of the residue is almost consistent with that of the commercial H_3BTC

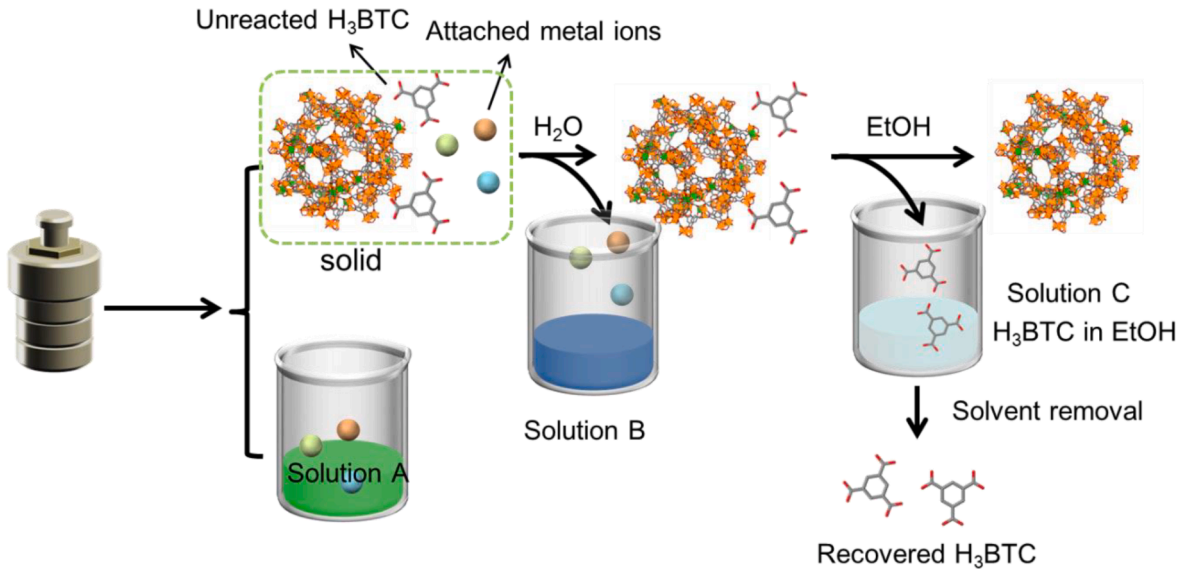

Scheme 2. The overall treatment route for the reaction products and unreacted raw materials.

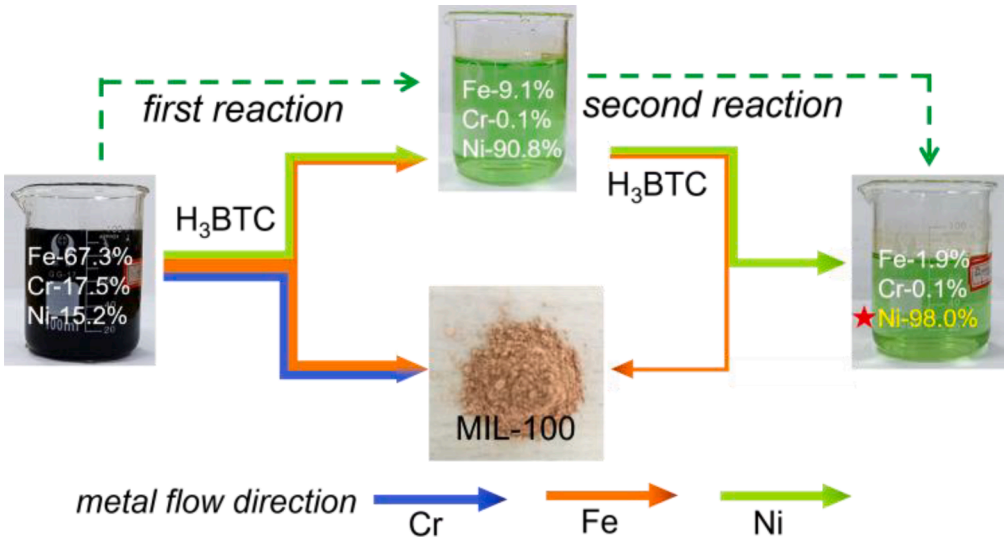

Scheme 3. The composition change and metal flow direction of the pickling wastewater during the two-step reactions with H3BTC.

reagent. Thus, we suggest the recovery of the unreacted H_3BTC ligands is feasible.

Besides, we measured the volume of Solution A, the metal concentrations of Solution A and B (Table S10). It was found the volume of Solution A is less than the original volume (20 mL). The reduced amount of water is attributed to several factors: crystal water (one crystal unit may contain 10~30 water molecules (Férey et al., 2004; Horcajada et al., 2007); coagulation in the top of cap of reaction bomb; adsorption on the surface and inside the channel; some losses during the operation process (e.g. centrifugation); and possible volatilization under high synthesis temperature and pressure. Based on the relevant calculation (presented in Scheme S1), we found that the molar ratios of reduced Fe/Cr ions in the wastewater are almost close to Fe/Cr ratio in the solid products; and the concentration of Ni^{2+} in Solution A is possibly higher than that in original solution. Corresponding description was presented in Supplementary Information.

3.6. Selective crystallization mechanism

As presented above, under the strongly acidic system, Ni hardly involved MIL-100 products whatever in the first-step reaction (C_{Ni} = 8918 mg/L, 15.2 wt%) or second-step reaction (C_{Ni} = 9210 mg/L, 90.8 wt%). That is, even with high concentration and very weak competition effect from Fe^{3+}/Cr^{3+}, the reaction activity of Ni^{2+} is rather lower in this strongly acid system. This fact indicates the weak interference of Ni^{2+} for Fe/Cr-MIL-100 formation. According to a metal-ligand covalency study by Hocking et al., (Hocking and Hambley, 2003) the high oxidation state of metal cation will increase the proportion of covalency bonds in the total metal-ligand interactions (including ionic and covalent interactions). This principle applies to our system: Fe^{3+}/Cr^{3+} will form more stable bonds and framework with carboxyl ligands than bivalent Ni^{2+}. Besides, Lewis acid/base theory suggests that high-charge Fe^{3+}/Cr^{3+} (strong Lewis acid) will react preferentially with the COO^- organic ligands (strong Lewis base) than low-charge Ni^{2+}. Thus, the selective crystallization mechanism can be cleared out.

3.7. Water-phase adsorption performances

Continuous development of industries including printing, dyeing, pharmacy, mining and smelting have caused the inevitable pollutions

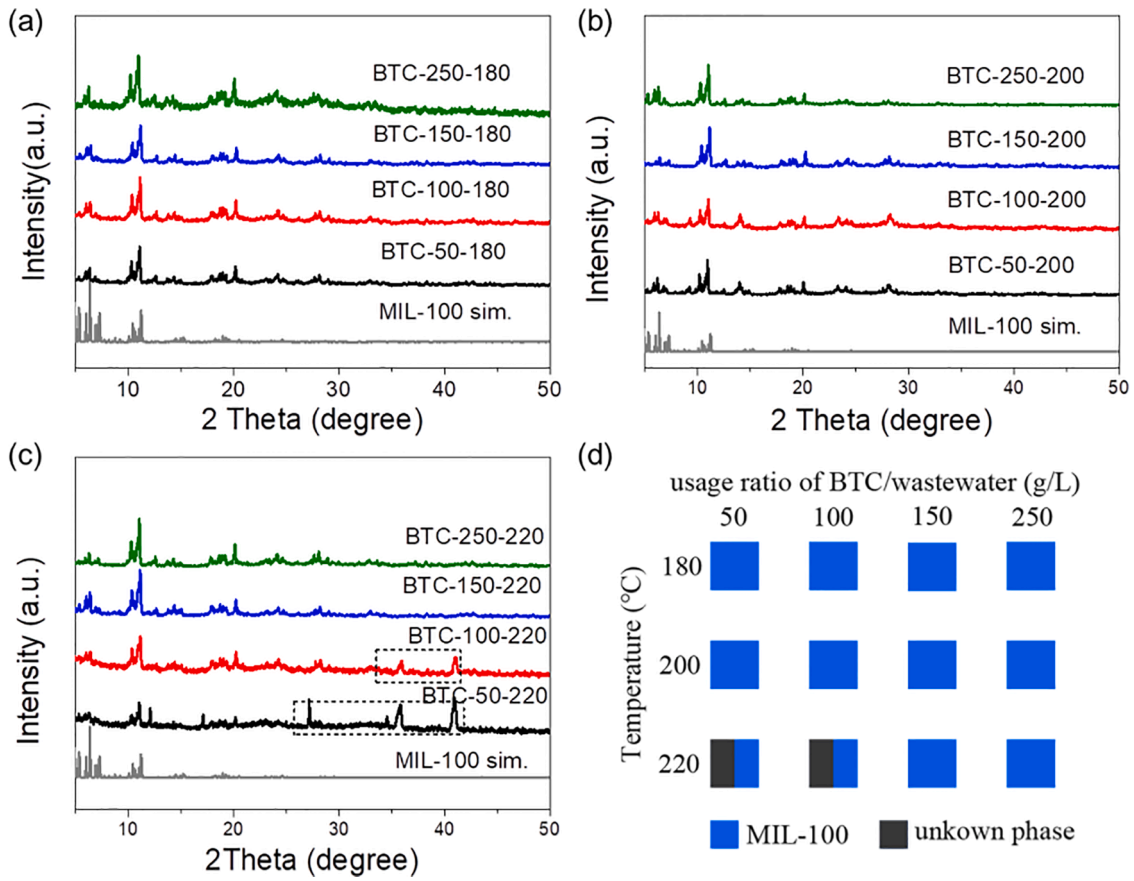

Fig. 1. (a–c) Powder XRD patterns and (d) crystal phase distribution of BTC-X-Y.

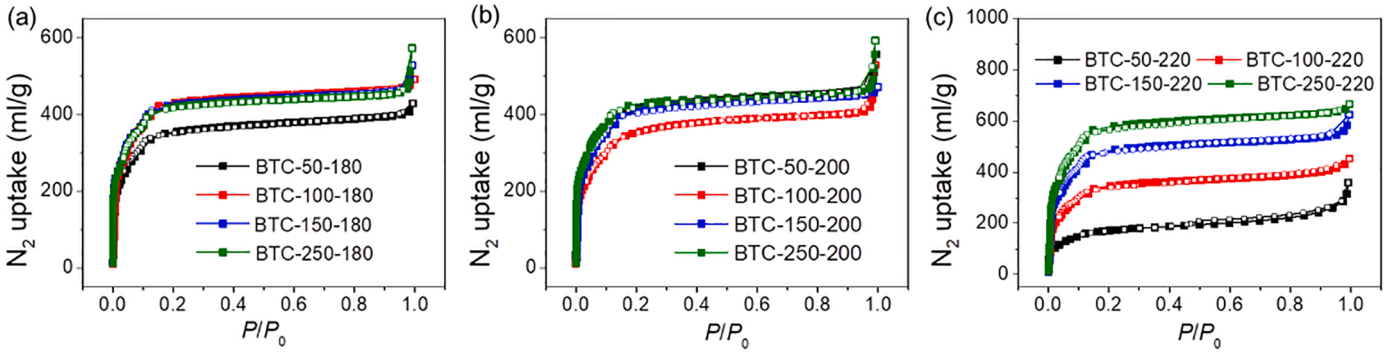

Fig. 2. N2 adsorption-desorption isotherms at 77 K of (a) BTC-X-180, (b) BTC-X-200 and (c) BTC-X-220 samples.

towards water resources. Therein, organic dye, antibiotic, and heavy metal ion are three common classes of pollutants. Due to the high stability and porosity, the water-phase adsorption performances of the BTC-X-Y products are desirable. We evaluated the adsorption performances of all the samples for MB dye, MOX antibiotic, and Zr(IV) ion. As shown in Fig. S21, BTC-250-180 exhibits largest adsorption capacities for all the pollutants among the products. To understand the difference, we measured the points of zero charge (pH_{pzc}, the pH where surface charge is zero) of the samples based on the solution pH change before and after addition of sample. As shown in Fig. S22–S24, all the samples are negatively charged at the pH range of 2.0~6.0, and the surface charge of BTC-250-180 is lowest. Thus, the electrostatic interaction of BTC-250-180 towards these cationic pollutants is stronger than other products. Some samples with similar specific surface areas but higher surface charges exhibit lower adsorption amounts. This further reflects the importance of surface charge (or electrostatic interaction). Besides, we found that the specific surface area is also an important factor to affect the adsorption amount. For example, BTC-250-220 shows comparable adsorption performances with BTC-250-180. Although the negative charge of this sample is weaker than BTC-250-180, the large specific surface area promotes its effective adsorption. As a comparison, BTC-50-220 with the poorest porosity shows the lowest adsorption amounts. Concluded above, we suggest the most important factors that affecting adsorption are specific surface area (or porosity) and surface charge property.

As the optimized product, BTC-250-180 was further investigated for its detailed adsorption performances. As shown in Fig. 6a, the adsorption capacity for MB reaches up to 648 mg/g, almost consistent with that of MIL-100(Fe) and MIL-100(Cr) prepared by traditional methods (Tong et al., 2013). And separation for MB and MO in the mixed solution also

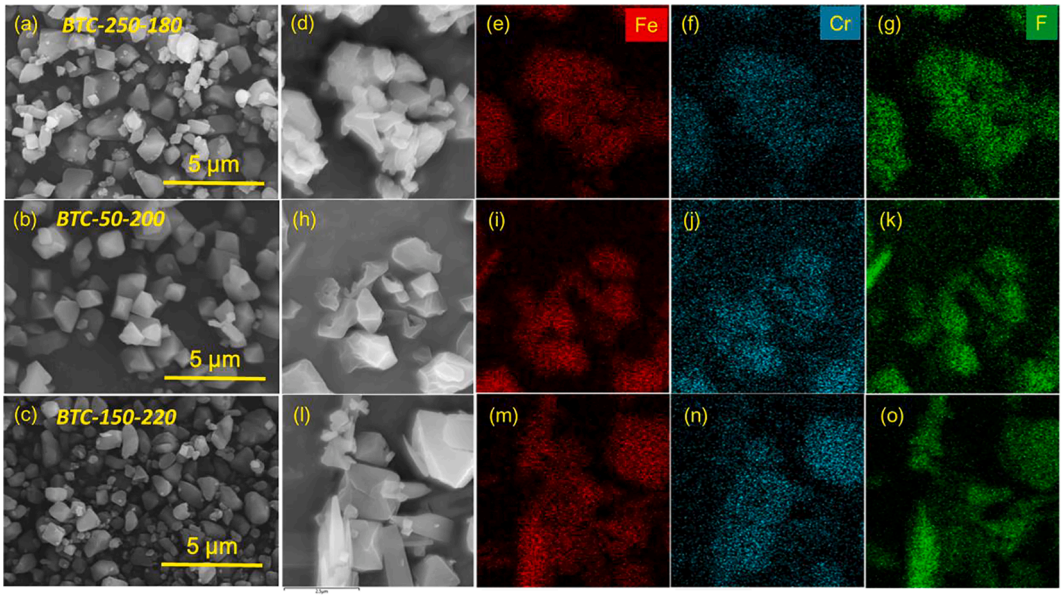

Fig. 3. SEM images of (a) BTC-250-180, (b) BTC-50-200 and (c) BTC-150-220; EDS mapping images of (d–g) BTC-250-180, (h–k) BTC-50-200 and (i–o) BTC-150-220.

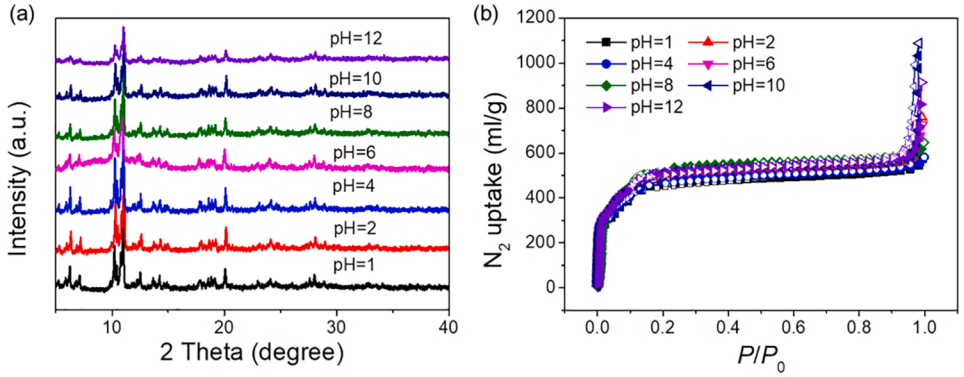

Fig. 4. (a) Powder XRD patterns and (b) N2 adsorption-desorption isotherms at 77 K of BTC-250–180 after being immersed in acid/base aqueous solutions for 10 days.

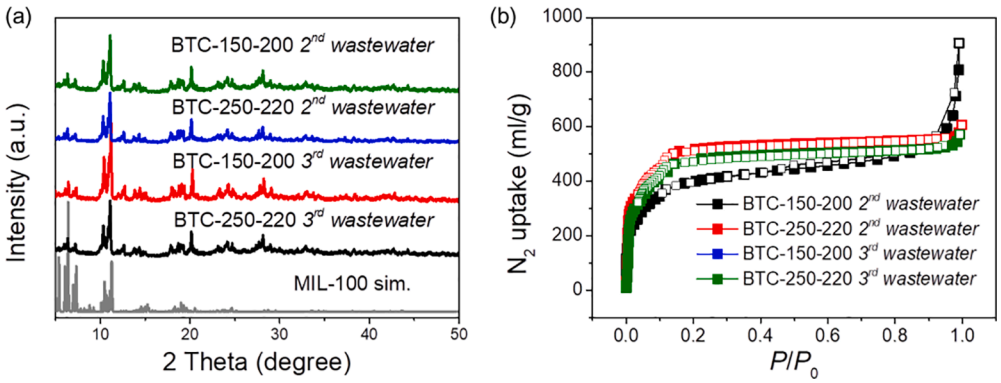

Fig. 5. (a) Powder XRD patterns and (b) N2 adsorption-desorption isotherms at 77 K of BTC-150-200 and BTC-250-220 prepared by 2nd and 3rd batches of wastewater.

proves to be feasible (Fig. 6b). Besides the dye, BTC-250-180 also exhibits high adsorption capacities of 496 and 202 mg/g for MOX antibiotic and Zr(IV) ion (Fig. 6c and d). We found the adsorption capacities of BTC-250-180 are higher than or close to that of reported MOFs and biomasses (Yang and Cannon, 2022; Afroze et al., 2016; Al-Ghouti and Al-Absi, 2020; Zhang et al., 2019; Haque et al., 2011; Akhtar et al., 2021; Li et al., 2020; Chai et al., 2019; Bhatti and Amin, 2013; Bhatti et al., 2016; Faghihian and Kabiri-Tadi, 2010; Hanif et al., 2015), as listed in Table S11. Thus, the pickling wastewater-resulted MIL-100 s may serve as potential adsorbents for cationic pollutants, and an idea "using waste

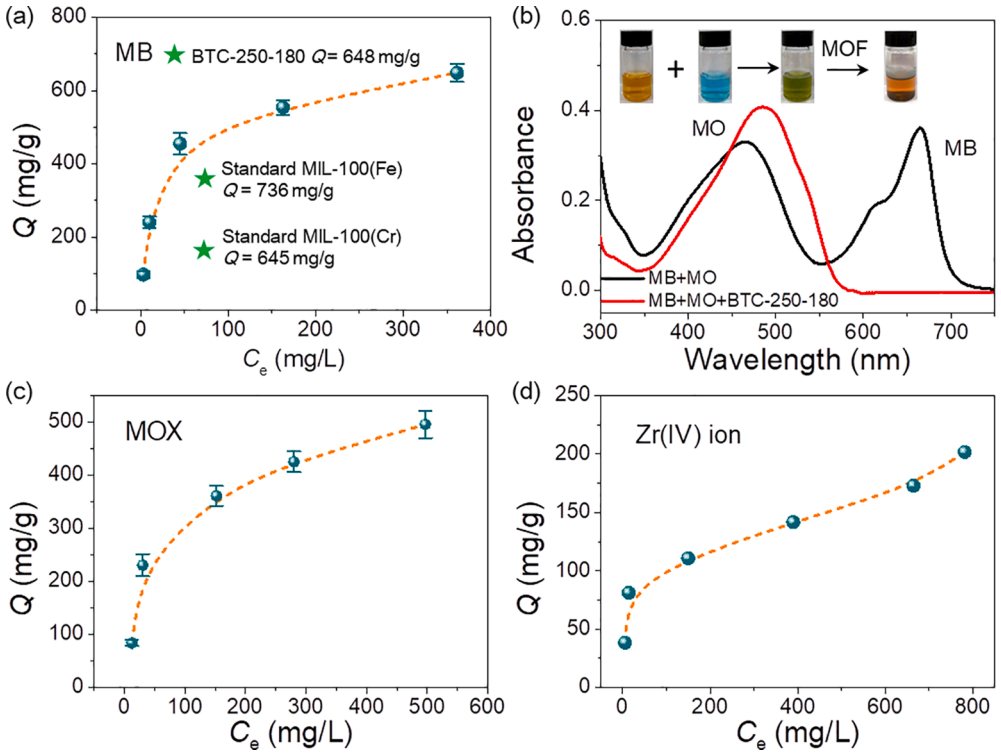

Fig. 6. Adsorption isotherms of BTC-250-180 sample for (a) MB, (c) MOX and (d) Zr(IV) ion adsorption; (b) UV-Vis spectra of MB-MO mixture before and after being treated by BTC-250-180 sample.

to treat waste" may be achieved.

3.8. Optimal synthesis condition for industrial production

As discussed above, under different reaction conditions, BTC-X-Y samples exhibit different porosities, yields, surface charges, adsorption performances, and synthesis costs. Herein, we recommended an optimal condition for potential industrial production: solid/liquid ratio (X), 250 g/L; temperature (Y), 180 °C. In other words, BTC-250-180 is the relatively ideal selection. The reasons for this suggestion are as follows:

(i) About adsorption performance: Among all the samples, BTC-250-180 exhibits the largest adsorption capacities for MB dye, MOX antibiotic, and Zr(IV) metal ion. From the view of adsorption performance, BTC-250-180 is the best choice.

(ii) About H_3BTC usage (X of BTC-X-Y): High H_3BTC usage (e.g. 250 g/L) seems not to be an optimal choice, due to the lower yield. However, based on the designed procedure (Scheme 2), the unreacted H_3BTC can be recovered and may further be used in subsequent synthesis process. Besides, with the increase of H_3BTC usage, the utilization efficiency of the metal ions can be increased largely, benefiting to the treatment of pickling wastewater.

(iii) About synthesis temperature (Y of BTC-X-Y): In this work, we only considered the cost of raw materials but not electric charge. In fact, the cost of industrial electricity is high and must be considered if produced in factories. Thus, the lower synthesis temperature (180 °C) will benefit to saving electricity and decreasing the production cost.

(iv) About porosity: Among all the samples, BTC-250-180 exhibits a high specific surface area (1341.2 m^2/g), comparable with most of other BTC-X-Y samples and those in the reported literatures.

(v) About purity: BTC-250-180 has a high purity of 95.6%, close to that of most of other BTC-X-Y samples.

4. Conclusion

In summary, we show that stainless steel pickling wastewater was easily transformed to Fe/Cr-MIL-100 and meanwhile Ni^{2+} can be largely purified. The use of raw-material-integrated pickling wastewater simplified the preparation process and decreased the costs of MOFs. The obtained MIL-100 s exhibit high porosity, long-term acid/base stability, and excellent water-phase adsorption performance. The Fe/Cr ratio was found to be controllable through modifying reaction temperature and solid/liquid ratio. More importantly, the formation of MIL-100 s from pickling wastewater was not largely controlled by the discharge batch of the wastewater. Thus, our work offers an industry-ready method to converse the liquid waste to high-value-added and low-cost products, facilitating the sustainable development of resource and environment.

CRediT authorship contribution statement

Xudong Zhao: Conceptualization, Investigation, Formal analysis, Writing – original draft, Funding acquisition. **Chengwei Zhang:** Methodology, Investigation. **Baosheng Liu:** Investigation, Formal analysis, Writing – review & editing, Funding acquisition. **Huifang Zhao:** Methodology, Investigation. **Xinli Gao:** Methodology, Funding acquisition. **Yuanyang Wang:** Methodology, Formal analysis. **Yuezhong Zhang:** Methodology, Formal analysis. **Dahuan Liu:** Conceptualization, Formal analysis, Writing – review & editing, Funding acquisition. **Chong-Chen Wang:** Conceptualization, Formal analysis, Writing – review & editing.

Declaration of Competing Interest

The authors declare that they have no known competing financial interests or personal relationships that could have appeared to influence the work reported in this paper.

Data Availability

Data will be made available on request.

Acknowledgments

This work was supported by Fundamental Research Program in Shanxi Province (No. 20210302124685 and 202103021223281), National Natural Science Foundation of China (No. 21978005), and Key Scientific Research Project in Shanxi Province (No. 202102050201003).

Supplementary materials

Supplementary material associated with this article can be found, in the online version, at doi:10.1016/j.resconrec.2022.106647.

References

Afroze, S., Sen, T.K., Ang, M., Nishioka, H., 2016. Adsorption of methylene blue dye from aqueous solution by novel biomass *Eucalyptus sheathiana* bark: equilibrium, kinetics, thermodynamics and mechanism. Desalin. Water Treat. 57, 5858–5878.

Akhtar, L., Ahmad, M., Iqbal, S., Abdelhafez, A.A., Mehran, M.T., 2021. Biochar's adsorption performance towards moxifloxacin and ofloxacin in aqueous solution: role of pyrolysis temperature and biomass type. Environ. Technol. Innov. 24, 101912.

Al-Ghouti, M.A., Al-Absi, R.S., 2020. Mechanistic understanding of the adsorption and thermodynamic aspects of cationic methylene blue dye onto cellulosic olive stones biomass from wastewater. Sci. Rep. 10, 15928.

Bezverkhyy, I., Weber, G., Bellat, J.-.P., 2016. Degradation of fluoride-free MIL-100(Fe) and MIL-53(Fe) in water: effect of temperature and pH. Micropor. Mesopor. Mater. 219, 117–124.

Bhatti, H.N., Amin, M., 2013. Removal of zirconium(IV) from aqueous solution by *Coriolus versicolor*: equilibrium and thermodynamic study. Ecol. Eng. 51, 178–180.

Bhatti, H.N., Zaman, Q., Kausar, A., Noreen, S., Iqbal, M., 2016. Efficient remediation of Zr(IV) using citrus peel waste biomass: kinetic, equilibrium and thermodynamic studies. Ecol. Eng. 95, 216–228.

Carraro, G., Gasparotto, A., Maccato, C., Barreca, D., 2013. Fluorine-doped iron oxide nanomaterials by plasma enhanced-CVD: an XPS study. Surf. Sci. Spectra 20, 9–16.

Chai, F., Zhao, X., Gao, H., Zhao, Y., Huang, H., Gao, Z., 2019. Effective removal of antibacterial drugs from aqueous solutions using porous metal-organic frameworks. J. Inorg. Organomet. P. 29, 1305–1313.

Dhakshinamoorthy, A., Alvaro, M., Hwang, Y.K., Seo, Y.-.K., Corma, A., Garcia, H., 2011. Intracrystalline diffusion in metal organic framework during heterogeneous catalysis: influence of particle size on the activity of MIL-100 (Fe) for oxidation reactions. Dalton Trans 40, 10719–10724.

European Comission. Reference document on best available techniques in the ferrous metal processing industry, 2001.

Faghihian, H., Kabiri-Tadi, M., 2010. Removal of zirconium from aqueous solution by modified clinoptilolite. J. Hazard. Mater. 178, 66–73.

Fathieh, F., Kalmutzki, M.J., Kapustin, E.A., Waller, P.J., Yang, J., Yaghi, O.M., 2018. Practical water production from desert air. Sci. Adv. 4, eaat3198.

Férey, G., Serre, C., Mellot-Draznieks, C., Millange, F., Surblé, S., Dutour, J., Margiolaki, I., 2004. A hybrid solid with giant pores prepared by a combination of targeted chemistry, simulation, and powder diffraction. Angew. Chem. Int. Ed. 43, 6296–6301.

Gross, T., Treu, D., 2008. Characterization of Cr(III) compounds of O, OH, F and Cl by XPS. Surf. Sci. Spectra 15, 77–123.

Guo, X.-.Z., Han, S.-.S., Yang, J.-.M., Wang, X.-.M., Chen, S.-.S., Quan, S., 2020. Effect of synergistic interplay between surface charge, crystalline defects, and pore volume of MIL-100(Fe) on adsorption of aqueous organic dyes. Ind. Eng. Chem. Res. 59, 2113–2122.

Hamon, L., Heymans, N., Llewellyn, P.L., Guillerm, V., Ghoufi, A., Vaesen, S., Maurin, G., Serre, C., De Weireld, G., Pirngruber, G.D., 2012. Separation of CO2-CH4 mixtures in the mesoporous MIL-100(Cr) MOF: experimental and modeling approaches. Dalton Trans 41, 4052–4059.

Hanif, A., Bhatti, H.N., Hanif, M.A., 2015. Removal of zirconium from aqueous solution by Ganoderma lucidum: biosorption and bioremediation studies. Desalin. Water Treat. 53, 195–205.

Haque, E., Jun, J.W., Jhung, S.H., 2011. Adsorptive removal of methyl orange and methylene blue from aqueous solution with a metal-organic framework material, iron terephthalate (MOF-235). J. Hazard. Mater. 185, 507–511.

Hasan, Z., Jeon, J., Jhung, S.H., 2012. Adsorptive removal of naproxen and clofibric acid from water using metal-organic frameworks. J. Hazard. Mater. 209, 151–157.

Hermose, J., Dufour, J., Gálvez, J.L., Negro, C., López-Mateos, F., 2005. Nickel hydroxide recovery from stainless steel pickling liquors by selective precipitation. Ind. Eng. Chem. Res. 44, 5750–5756.

Hocking, R.K., Hambley, T.W., 2003. Structural measure of metal-ligand covalency from the bonding in carboxylate ligands. Inorg. Chem. 42, 2833–2835.

Horcajada, P., Surblé, S., Serre, C., Hong, D.-.Y., Seo, Y.-.K., Chang, J.-.S., Grenèche, J.-.M., Margiolaki, I., Férey, G., 2007. Synthesis and catalytic properties of MIL-100(Fe), an iron(III) carboxylate with large pores. Chem. Commun. 2820–2822.

Huo, S.-.H., Yan, X.-.P., 2012. Metal-organic framework MIL-100(Fe) for the adsorption of malachite green from aqueous solution. J. Mater. Chem. 22, 7449–7455.

Jhung, S.H., Lee, J.-.H., Chang, J.-.S., 2005. Microwave synthesis of a nanoporous hybrid materials, chromium trimesate. Bull. Korean Chem. Soc. 26, 880–881.

Jing, P., Wu, B., Han, Z., Shi, W., Cheng, P., 2021. An efficient Ag/MIL-100(Fe) catalyst for photothermal conversion of CO_2 at ambient temperature. Chin. Chem. Lett. 32, 3505–3508.

Kabtamu, D.M., Wu, Y.-.N., Chen, Q., Zheng, L., Otake, K.-.I., Matović, L., Li, F., 2020. Facile upcycling of hazardous Cr-containing electroplating sludge into value-added metal-organic frameworks (MOFs) for efficient adsorptive desulfurization. ACS Sustain. Chem. Eng. 8, 12443–12452.

Li, Y.-.X., Wang, L., Chai, F.-.F., Jing, H.-.F., Gao, Z.-.Q., Zhang, Q.-.H., Zhao, X.-.D., 2020. Highly effective removal of antibiotics from aqueous solution by magnetic $ZnFe_2O_4$/activated carbon composite. Water Sci. Technol. 82, 877–886.

Lian, X., Feng, D., Chen, Y.-.P., Liu, T.-.F., Wang, X., Zhou, H.-.C., 2015. The preparation of an ultrastable mesoporous Cr(III)-MOF via reductive labilization. Chem. Sci. 6, 7044–7068.

Long, P., Wu, H., Zhao, Q., Wang, Y., Dong, J., Li, J., 2011. Solvent effect on the synthesis of MIL-96(Cr) and MIL-100(Cr). Micropor. Mesopor. Mater. 142, 489–493.

Perez, E., Amador, R.N., Carboni, M., Meyer, D., 2016. In-situ precipitation of metal-organic frameworks from a simulant battery waste solution. Mater. Letter. 167, 188–191.

Plaza, M.G., Ribeiro, A.M., Ferreira, A., Santos, J.C., Hwang, Y.K., Seo, Y.-.K., Lee, U.-.H., Chang, J.-.S., Loureiro, J.M., Rodrigues, A.E., 2012. Separation of C3/C4 hydrocarbon mixtures by adsorption using a mesoporous iron MOF: MIL-100(Fe). Micropor. Mesopor. Mater 153, 178–190.

Razavi, S.A.A., Morsali, A., 2020. Metal ion detection using luminescent-MOFs: principles, strategies and roadmap. Coordin. Chem. Rev. 415, 213299.

Rögener, F., Sartor, M., Bán, A., Buchloh, D., Reichardt, T., 2012. Metal recovery from spent stainless steel pickling solutions. Resour. Conserv. Recy. 60, 72–77.

Song, K., Qiu, X., Han, B., Liang, S., Lin, Z., 2021. Efficient upcycling electroplating sludge and waste PET into Ni-MOF nanocrystals for the effective photoreduction of CO_2. Environ. Sci. Nano 8, 390–398.

Tan, F., Liu, M., Li, K., Wang, Y., Wang, J., Guo, X., Zhang, G., Song, C., 2015. Facile synthesis of size-controlled MIL-100(Fe) with excellent adsorption capacity for methylene blue. Chem. Eng. J. 281, 360–367.

Tong, M., Liu, D., Yang, Q., Devautour-Vinot, S., Maurin, G., Zhong, C., 2013. Influence of framework metal ions on the dye capture behavior of MIL-100 (Fe, Cr) MOF type solids. J. Mater. Chem. A 1, 8534–8537.

Valenzano, L., Civalleri, B., Chavan, S., Bordiga, S., Nilsen, M.H., Jakobsen, S., Lillerud, K.P., Lamberti, C., 2011. Disclosing the complex structure of UiO-66 metal organic framework: a synergic combination of experiment and theory. Chem. Mater. 23, 1700–1718.

Vo, T.K., Kim, J.-.H., Kwon, H.T., Kim, J., 2019. Cost-effective and eco-friendly synthesis of MIL-101(Cr) from waste hexavalent chromium and its application for carbon monoxide separation. J. Ind. Eng. Chem. 80, 345–351.

Wickenheisser, M., Jeremias, F., Henninger, S.K., Janiak, C., 2013. Grafting of hydrophilic ethylene glycols or ethylenediamine on coordinatively unsaturated metal sites in MIL-100(Cr) for improved water adsorption characteristics. Inorg. Chim. Acta 407, 145–152.

Xia, T., Lin, Y., Li, W., Ju, M., 2021. Photocatalytic degradation of organic pollutants by MOFs based materials: a review. Chin. Chem. Lett. 32, 2975–2984.

Yang, S., Li, W., Zhang, H., Wen, Y., Ni, Y., 2019. Treatment of paper mill wastewater using a composite inorganic coagulant prepared from steel mill waste pickling liquor. Sep. Purif. Technol. 209, 238–245.

Yang, Y., Cannon, F.S., 2022. Biomass activated carbon derived from pine sawdust with steam bursting pretreatment; perfluorooctanoic acid and methylene blue adsorption. Bioresour. Technol 344, 126161.

Yi, Y., Tu, G., Ying, G., Fang, Z., Tsang, E.P., 2021. Magnetic biochar derived from rice straw and stainless pickling waste liquor for highly efficient adsorption of crystal violet. Bioresour. Technol 341, 125743.

Yoon, J.W., Seo, Y.-.K., Hwang, Y.K., 2010. Controlled reducibility of a metal-organic framework with coordinatively unsaturated sites for preferential gas sorption. Angew. Chem. Int. Ed. 49, 5949–5952.

Zeng, H., Xie, M., Wang, T., Wei, R.-.J., Xie, X.-.J., Zhao, Y., Lu, W., Li, D., 2021. Orthogonal-array dynamic molecular sieving of propylene/propane mixtures. Nature 595, 542–548.

Zhang, L., Li, R., Zhou, L., Li, Q., Dong, F., Yan, Y., 2021. Recycling the steel pickling waste liquor to produce a low-cost material for immobilization of heavy metal(loid) s. Environ. Technol. Inno. 24, 102001.

Zhang, W., Yang, J.-.M., Yang, R.-.N., Yang, B.-.C., Quan, S., Jiang, X., 2019. Effect of free carboxylic acid groups in UiO-66 analogues on the adsorption of dyes from water: plausible mechanisms for adsorption and gate-opening behavior. J. Mol. Liq. 283, 160–166.